Adv Comput Math (2017) 43:295–318
DOI 10.1007/s10444-016-9486-8

Microlocal analysis of edge flatness through directional multiscale representations

Kanghui Guo[1] · **Demetrio Labate**[2]

Received: 23 September 2015 / Accepted: 4 October 2016 /
Published online: 12 October 2016

Abstract Edges and surface boundaries are often the most relevant features in images and multidimensional data. It is well known that multiscale methods including wavelets and their more sophisticated multidimensional siblings offer a powerful tool for the analysis and detection of such sets. Among such methods, the continuous shearlet transform has been especially successful. This method combines anisotropic scaling and directional sensitivity controlled by shear transformations in order to precisely identify not only the location of edges and boundary points but also edge orientation and corner points. In this paper, we show that this framework can be made even more flexible by controlling the scaling parameter of the anisotropic dilation matrix and considering non-parabolic scaling. We prove that, using 'higher-than-parabolic' scaling, the modified shearlet transform is also able to estimate the degree of local flatness of an edge or surface boundary, providing more detailed information about the geometry of edge and boundary points.

Keywords Analysis of singularities · Continuous wavelets · Curvelets · Directional wavelets · Edge detection · Shearlets · Wavelets

Mathematics Subject Classification (2010) 42C15 · 42C40 · 65T60

Communicated by: Yang Wang

✉ Demetrio Labate
dlabate@math.uh.edu

Kanghui Guo
KanghuiGuo@MissouriState.edu

[1] Missouri State University, Springfield, MO 65804, USA

[2] University of Houston, Houston, TX 77204, USA

1 Introduction

One of the most salient properties of the continuous wavelet transform is its sensitivity to the local regularity of functions and distributions. If f is a function that is smooth apart from a discontinuity at a point p_0, the continuous wavelet transform of f, denoted by $\mathcal{W}f(a, p)$, signals the location of the discontinuity through its decay rate as the scale variable a approaches 0 (the asymptotic decay is fast unless p is near p_0 [16, 23]). More generally, the continuous wavelet transform is able to resolve the singular support of f and to measure the pointwise regularity of functions [17, 18].

It is also known that the conventional wavelet approach offers rather limited capabilities for the analysis of the *geometry* of the singularity set. For example, it cannot detect the orientation of a singularity curve [15]. The continuous shearlet transform [20] was introduced with the goal of refining the microlocal properties of the conventional wavelet transform, and in fact is able to resolve the wavefront set of distributions [8, 20]. It was next shown in a sequence of more recent papers that the continuous shearlet transform provides a precise characterization of the local orientation of edges for a large class of multidimensional functions and distributions [9–11, 14, 21]. In particular, let us consider a function on $\mathbb{R}^2$ of the form $h = \sum_{i=1}^{N} c_i \chi_{S_i}$, where, for each i, c_i is a constant and S_i is a compact subset of $\mathbb{R}^2$ with a piecewise regular boundary ∂S_i. The continuous shearlet transform characterizes the *location* and *orientation* of the boundary curves ∂S_i through its asymptotic decay properties at finer scales; this result includes the characterization of corner points. Similar results hold true for more general piecewise smooth functions [13] and in the three-dimensional setting [10, 11], and provide the theoretical underpinning for highly competitive numerical algorithms of edge detection and feature extraction in image processing applications [5, 6, 22, 24–27].

In this paper, we show that the shearlet framework can be applied to detect and analyze an additional property of edges, namely the *edge flatness*. This property enables one to distinguish, for example, a circular edge from a linear edge through the local asymptotic decay of the shearlet transform at edge points. Up to the knowledge of the authors, this is the first result of this type to appear in the literature and it is based on a novel application of the shearlet framework, where *the scaling parameter of the dilation matrix need to be chosen 'higher-than-parabolic'* (the precise definition will be given below). This result is both of theoretical and practical interest. On the theoretical side, it is remarkable that the standard shearlet transform based on parabolic scaling is not sensitive to the edge flatness, and that *non-parabolic (anisotropic) scaling is required* for this task. The proof of this new result adapts the general organization of the proofs in [9] (for the 2D case) and [11] (for the 3D case); however the main argument used for the most critical part of the proof, namely the part dealing with the 'slow-decaying' terms in the edge detection estimate, is new. On the practical side, this new result suggests that discrete multiscale directional transforms could potentially take advantage of non-parabolic scaling to encode more informative and discriminating features of imaging data. Even though the actual implementation of this idea is beyond the scope of this paper, a very simple numerical experiment reported below indicates that this idea is feasible.

We also recall that the analysis of singularities is related to the so-called geometric separation problem [4], aiming at separating into geometrically distinct components functions or distributions containing different types of singularities, e.g., point, lines and curve singularities. It was shown that the microlocal properties of the continuous shearlet [12] and curvelet transforms [4] are critical to separate different types of singularities, and these results are the groundwork for powerful numerical algorithms for image inpainting [7, 19]. The new ideas presented this paper could potentially extend the current results allowing for the separation of curve singularities with different flatness properties, e.g., linear and non-linear singularities.

We finally remark that historically the idea of using wavelet-like transforms to perform microlocal analysis is older than wavelets and can be traced back to the FBI transform of Bros and Iagolnitzer [1] and the wave packets by Cordoba and Fefferman [3]. These methods define implicitly a kind of anisotropic scaling and were shown to be able to resolve the wavefront set of distributions. The curvelet and shearlet transforms were introduced more recently and can be seen as a refinement and more flexible versions of these older transforms. We refer to [2] for a more detailed discussion of the comparison between these various ideas.

1.1 Paper organization

The rest of the paper is organized as follows. In Section 2, we recall the definition of the continuous shearlet transform and its main properties and introduce the version of the continuous shearlet transform that will be used in this paper. In Section 3, we present our main result about the shearlet characterization of the local flatness of edge points in functions of two variables. In Section 4, we extend the result from Section 3 to the 3-dimensional setting.

2 The continuous shearlet transform in $\mathbb{R}^2$

We briefly recall below the definition and main properties of the continuous shearlet transform, originally introduced in [20].

2.1 Continuous shearlets in the plane

For a fixed $0 \leq \beta < 1$, a *continuous shearlet system* generated by $\psi \in L^2(\mathbb{R}^2)$ is a collection of functions of the form

$$\left\{\psi_{a,s,p}(x) = |\det M(a,s)|^{-\frac{1}{2}}\psi(M(a,s)^{-1}(x-p)) : a > 0, s \in \mathbb{R}, p \in \mathbb{R}^2\right\}, \tag{1}$$

where the matrix $M(a,s)$ is either $M_h(a,s) = \begin{pmatrix} a & -a^\beta s \\ 0 & a^\beta \end{pmatrix}$ or $M_v(a,s) = \begin{pmatrix} a^\beta & 0 \\ -a^\beta s & a \end{pmatrix}$.

It is easy to verify that $M_h(a,s)$ can be factored out as the product $B(s)\,A(a)$ of the *anisotropic dilation matrix* $A(a) = \begin{pmatrix} a & 0 \\ 0 & a^\beta \end{pmatrix}$ and the *shear matrix* $B(s) = \begin{pmatrix} 1 & -s \\ 0 & 1 \end{pmatrix}$. A similar factorization holds for $M_v(a,s)$. When $\beta = 1/2$, the anisotropic dilation matrix $A(a)$ is associated with the so-called *parabolic scaling*, meaning that the action of $A(a)$ on elements of $\mathbb{R}^2$ produces a scaling that, along one coordinate axis, is quadratic with respect to the other coordinate direction. The parabolic scaling is the standard choice in the classical theory of curvelets [2] and shearlets [20]. The scaling becomes increasingly more anisotropic when $\beta < 1/2$ and less anisotropic when $\beta > 1/2$. In the limiting case where $\beta = 1$, then $A(a)$ is the (isotropic) dyadic dilation matrix, which is used in classical wavelets. The other limiting case, where $\beta = 0$, corresponds to the situation of 'extreme' anisotropic scaling where dilation occurs along one coordinate axis only.

For appropriate choices of the generator function ψ, the continuous shearlets are associated with a continuous reproducing formula. More precisely, let $\psi^{(h)}, \psi^{(v)} \in L^2(\mathbb{R}^2)$ be given by in the Fourier domain by

$$\hat{\psi}^{(h)}(\xi_1,\xi_2) = \hat{\psi}_1(\xi_1)\,\hat{\psi}_2\Big(\frac{\xi_2}{\xi_1}\Big), \quad \hat{\psi}^{(v)}(\xi_1,\xi_2) = \hat{\psi}_1(\xi_2)\,\hat{\psi}_2\Big(\frac{\xi_1}{\xi_2}\Big), \tag{2}$$

where $\xi = (\xi_1,\xi_2) \in \mathbb{R}^2$. Correspondingly, we define the *horizontal* and *vertical continuous shearlets* by

$$\psi^{(h)}_{a,s,p}(x) = |\det M_h(a,s)|^{-\frac{1}{2}}\psi^{(h)}(M_h(a,s)^{-1}(x-p)), \quad a>0, s\in\mathbb{R}, p\in\mathbb{R}^2,$$

and

$$\psi^{(v)}_{a,s,p}(x) = |\det M_v(a,s)|^{-\frac{1}{2}}\psi^{(v)}(M_v(a,s)^{-1}(x-p)), \quad a>0, s\in\mathbb{R}, p\in\mathbb{R}^2,$$

respectively. The following proposition is a simple extension of a result from [20] (the original proof for $\beta = 1/2$ extends almost verbatim to the case of general $0 \le \beta \le 1$).

Proposition 1 *Let $\psi^{(d)} \in L^2(\mathbb{R}^2)$, for $d \in \{h,v\}$, be given by* Eq. 2, *where ψ_1, $\psi_2 \in L^2(\mathbb{R})$ satisfy the conditions*

$$\int_0^\infty |\hat{\psi}_1(a\omega)|^2\frac{da}{a} = 1, \text{ for a.e. } \omega\in\mathbb{R}; \quad \|\psi_2\|_2 = 1. \tag{3}$$

Then any $f \in L^2(\mathbb{R}^2)$ satisfies the formula

$$f = \int_{\mathbb{R}^2}\int_{\mathbb{R}}\int_0^\infty \langle f, \psi^{(d)}_{a,s,p}\rangle\,\psi^{(d)}_{a,s,t}\,\frac{da}{a^3}\,ds\,dp, \tag{4}$$

where the equality is understood in the L^2 sense.

In many applications, it is useful to impose additional assumptions on the functions ψ_1, ψ_2 in Eq. 2, to improve the localization properties of the shearlets $\psi^{(h)}_{a,s,p}$. Namely, both functions are assumed to be C^∞_c in the Fourier domain with

$$\text{supp}\,\hat{\psi}_1 \subset \left[-2, -\frac{1}{2}\right] \cup \left[\frac{1}{2}, 2\right] \text{ and supp}\,\hat{\psi}_1 \subset [-1, 1].$$

In this case, by writing the continuous horizontal shearlets in the Fourier domain as

$$\hat{\psi}^{(h)}_{a,s,p}(\xi_1, \xi_2) = a^{\frac{1+\beta}{2}}\,\hat{\psi}_1(a\,\xi_1)\,\hat{\psi}_2\left(a^{\beta-1}\left(\frac{\xi_2}{\xi_1} - s\right)\right) e^{-2\pi i \xi \cdot p},$$

it follows by the assumptions on ψ_1 and ψ_2 that the functions $\hat{\psi}^{(h)}_{a,s,p}$ have supports:

$$\text{supp}\,\hat{\psi}^{(h)}_{a,s,p} \subset \left\{(\xi_1, \xi_2) : \xi_1 \in \left[-\frac{2}{a}, -\frac{1}{2a}\right] \cup \left[\frac{1}{2a}, \frac{2}{a}\right],\ |\frac{\xi_2}{\xi_1} - s| \le a^{1-\beta}\right\}.$$

That is, the support of $\hat{\psi}^{(h)}_{a,s,p}$ is a pair of trapezoids, symmetric with respect to the origin, oriented along a line of slope s. The trapezoidal supports becomes increasingly more elongated as $a \to 0$. Very similar properties hold for the continuous vertical shearlets. In summary, the continuous shearlets form a collection of well-localized functions ranging over a multitude of scales, orientations and locations, associated with the variable a, s and p, respectively. The action of anisotropic dilations and shear matrices is illustrated in Fig. 1.

Using the horizontal and vertical shearlets, we define the *(fine-scale) continuous shearlet transform* on $L^2(\mathbb{R}^2)$ as the mapping

$$f \in L^2(\mathbb{R}^2 \setminus [-2, 2]^2)^\vee \to \mathcal{SH}_\psi f(a, s, p), \quad a \in \left(0, \frac{1}{4}\right], s \in [-\infty, \infty], p \in \mathbb{R}^2,$$

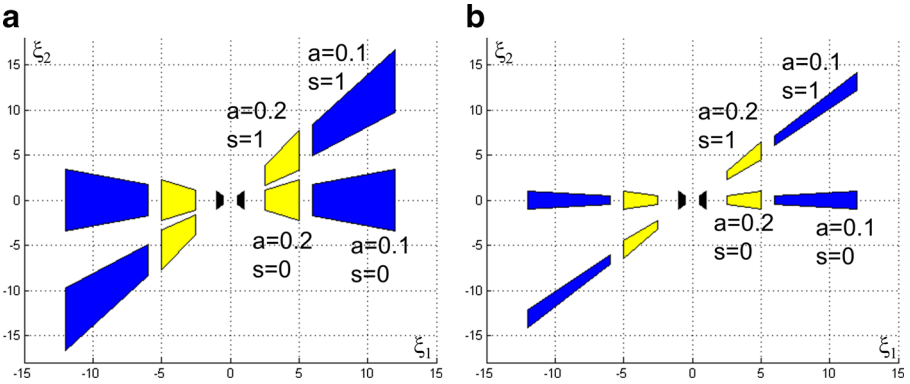

Fig. 1 Anisotropic scaling. The image shows the effect of the anisotropic scaling matrix $A(a)$ and the shear matric $B(s)$, for $a = 0.2$ and 0.1, $s = 0$ and $s = 1$, on the support region (*in black*) of the shearlet generator $\hat{\psi}^{(h)}$ (in the Fourier domain) using different values of the anisotropy parameter β. *Left panel*: $\beta = \frac{1}{2}$ (parabolic scaling); *right panel*: $\beta = 0$

given by

$$\mathcal{SH}_\psi f(a,s,p) = \begin{cases} \mathcal{SH}_\psi^{(h)} f(a,s,p) = \langle f, \psi_{a,s,p}^{(h)} \rangle, & \text{if } |s| \le 1 \\ \mathcal{SH}_\psi^{(v)} f(a,\frac{1}{s},p) = \langle f, \psi_{a,s,p}^{(v)} \rangle, & \text{if } |s| > 1. \end{cases}$$

In this expression, it is understood that the limit value $s = \pm\infty$ is defined and that $\mathcal{SH}_\psi f(a,\pm\infty,p) = \mathcal{SH}_\psi^{(v)} f(a,0,p)$.

The term *fine-scale* refers to the fact that this shearlet transform is only defined for the scale variable $a \in (0, 1/4]$, corresponding to "fine scales". In fact, for this range of scales, the shearlet transform $\mathcal{SH}_\psi f$ defines an isometry on $L^2(\mathbb{R}^2 \backslash [-2,2]^2)^\vee$, the subspace of $L^2(\mathbb{R}^2)$ of functions with Fourier-domain support away from $[-2,2]^2$, but not on $L^2(\mathbb{R}^2)$. This is not a limitation since the shearlet-based analysis of singularities we will present below is based on asymptotic estimates, as a approaches 0. In the following, for brevity, we will drop the wording 'fine-scale' and, henceforth, simply refer to this transform as the *continuous shearlet transform*.

2.2 Non-parabolic scaling and edge flatness

Results available in the literature about shearlet-based analysis of singularities set the anisotropy parameter as $\beta = 1/2$ in the definition of the matrix $M(a,s)$. The same assumption $\beta = 1/2$ is made for curvelets in [2] and also for the recently proposed approach in [21], that uses compactly supported shearlets. This choice of β is appropriate for the detection of the location and orientation of the edge points. Indeed, as it was observed in [14], other choices of $\beta \in (0,1)$ are possible and would also allow to detect the location and orientation of edges so that there is (apparently) no advantage in using a different β. The new observation we make in this paper is that, by choosing $0 \le \beta < 1/2$ in the continuous shearlet transform, we are able to detect the degree of flatness of an edge curve; this is not true if $\beta = 1/2$. The critical difference is that, when $\beta = 1/2$, the asymptotic decay rate of the continuous shearlet transform at an edge point p_0, for s corresponds to the normal direction at p_0, is of the order $(a^{3/4})$ *independently of the flatness of the edge* at p_0. By contrast, when $0 \le \beta < 1/2$, the asymptotic decay rate for the same values of p_0 and s is *dependent on the flatness of the edge at* p_0*, so that it is possible to distinguish edge points with different flatness by their asymptotic decay.*

In the following, to simplify notation and avoid making the arguments more technical, we will choose the special value $\beta = 0$ in the definition of the matrix $M(a,s)$ (other choices of $\beta \in (0,1/2)$ give a similar result). Therefore, henceforth we assume $\beta = 0$ so that $M_h(a,s) = \begin{pmatrix} a & -s \\ 0 & 1 \end{pmatrix}$ and $M_v(a,s) = \begin{pmatrix} 1 & 0 \\ -s & a \end{pmatrix}$. We will make a similar assumption for the 3D case in Section 4.

3 Shearlet analysis of piecewise smooth edges in the plane

In this section, we show that the continuous shearlet transform (with $\beta = 0$) provides a precise geometric characterization for the piecewise smooth edge of a planar region,

including its flatness. Before presenting our main theorems, we define below the class of functions we will consider and the notion of flatness.

3.1 Our 2D image model

As an idealized model of images with edges, we consider functions of the form $f = \sum_i \chi_{S_i}$, where the sets $S_i \subset \mathbb{R}^2$ are compact and disjoint ($S_i \cap S_j = \emptyset$ if $i \neq j$), and their boundary curves, denoted by ∂S_i, are smooth except possibly for finitely many corner points. To define the notion of a *corner point*, let $\boldsymbol{\alpha}(t)$ be the parametrization of a boundary curve ∂S with respect to the arc length parameter t. For any $t_0 \in (0, L)$ and any $j \geq 0$, we assume that $\lim_{t \to t_0^-} \boldsymbol{\alpha}^{(j)}(t) = \boldsymbol{\alpha}^{(j)}(t_0^-)$ and $\lim_{t \to t_0^+} \boldsymbol{\alpha}^{(j)}(t) = \boldsymbol{\alpha}^{(j)}(t_0^+)$ exist. Also, let $\mathbf{n}(t^-)$, $\mathbf{n}(t^+)$ be the outer normal direction(s) of ∂S at $\boldsymbol{\alpha}(t)$ from the left and right, respectively; if they are equal, we write them as $\mathbf{n}(t)$. Similarly, for the curvature of ∂S, we use the notation $\kappa(t^-)$, $\kappa(t^+)$ and $\kappa(t)$. We say that $p = \boldsymbol{\alpha}(t_0)$ is a *corner point of* ∂S if: either (i) $\boldsymbol{\alpha}'(t_0^-) \neq \pm\boldsymbol{\alpha}'(t_0^+)$ or (ii) $\boldsymbol{\alpha}'(t_0^-) = \pm\boldsymbol{\alpha}'(t_0^+)$, but $\kappa(t_0^-) \neq \kappa(t_0^+)$. When (i) holds, we say that p is a *corner point of first type* and, when (ii) holds, we say that p is a *corner point of second type*. On the other hand, if $\boldsymbol{\alpha}(t)$ is infinitely many times differentiable at t_0, we say that $\boldsymbol{\alpha}(t_0)$ is a *regular point* of ∂S. The boundary curve $\boldsymbol{\alpha}(t)$ is *piecewise smooth* if the values $\boldsymbol{\alpha}(t)$ are regular points for all $0 \leq t \leq L$, except for finitely many corner points.

Note that it is not necessary to require infinite regularity. We can replace the piecewise *smooth* boundary with a piecewise *regular* boundary of finite order, say C^m (for sufficiently large m), and derive a result similar to the one below at the cost of heavier notation. To keep notation simpler, we will only examine the case of piecewise smooth boundaries below.

3.2 Definition of flatness

Let $y = f(x)$, $a < x < b$, be a section of a smooth boundary curve ∂S of a planar region $S \subset \mathbb{R}^2$. Given $x_0 \in (a, b)$, via a translation and a rotation of the coordinates, we may assume that $f(x_0) = 0$, $f'(x_0) = 0$. If there exists a $k \geq 2$ such that $f^{(m)}(x_0) = 0$ for $0 \leq m \leq k-1$ and $f^{(k)}(x_0) \neq 0$, we say that the curve is *k-flat* (or that its *degree of flatness* is k) at $p_0 = (x_0, f(x_0))$. If no such k exists at p_0, we say that the boundary curve is ∞-*flat* at p_0. In this case, we assume that ∂S has the finite type property at p_0 in the sense that if $f^{(m)}(x_0) = 0$ for all $m \geq 2$, then ∂S is a line segment near p_0. For example, if S is a polygonal planar region, then the boundary curve ∂S is ∞-flat at each point that is not a corner point. If S is a compact region whose boundary has nonvanishing curvature everywhere (e.g., a disk), then the boundary curve is 2-flat at each point. Clearly, a larger k at p_0 means a flatter boundary at p_0.

We can extend the notion of flatness at a corner point using right- and left-derivatives. That is, given $y = f(x)$, $a < x \leq x_0$, via a translation and a rotation of the coordinates, we may assume that $f(x_0) = 0$, $f'(x_0^-) = 0$. If there exists a $k \geq 2$ such that $f^{(m)}(x_0^-) = 0$ for $0 \leq m \leq k-1$ and $f^{(k)}(x_0^-) \neq 0$, we say that

the curve is *left-k-flat* at $p_0 = (x_0, f(x_0)$ or that its degree of left-flatness is k. If no such k exists at p_0, we say that the curve is *left-∞-flat* at p_0. Similarly, for a function $y = f(x)$, $x_0 \le x < b$, we define right-flatness by using the right-derivative $f^{(m)}(x_0^+)$.

3.3 Main theorems (2D case)

Let $p_0 = \boldsymbol{\alpha}(t_0)$ be a regular point and let $s_0 = \tan(\theta_0)$ with $\theta_0 \in (-\frac{\pi}{2}, \frac{\pi}{2})$. Let $\Theta(\theta_0) = [\cos\theta_0, \sin\theta_0]$. We say that s_0 *corresponds to the normal direction of* ∂S *at* p_0 if $\Theta(\theta_0) = \pm\mathbf{n}(t_0)$. When $\boldsymbol{\alpha}(t_0)$ is a corner point, we can identify two outer normal directions $\boldsymbol{n}(t_0^-)$ and $\boldsymbol{n}(t_0^+)$.

We are now ready to state our main results. The first theorem below characterizes regular edge points; the second one deals with then presence of corner points.

Theorem 1 *Let $B = \chi_S$, where $S \subset \mathbb{R}^2$ is compact and its boundary, denoted by ∂S, is a simple curve, of finite length L, that is smooth except possibly for finitely many corner points. Let ψ_1, ψ_2 be chosen such that*

- $\hat{\psi}_1 \in C_c^\infty(\mathbb{R})$, *supp* $\hat{\psi}_1 \subset [-2, -\frac{1}{2}] \cup [\frac{1}{2}, 2]$, *is odd, nonnegative on* $[\frac{1}{2}, 2]$ *and it satisfies* $\int_0^\infty |\hat{\psi}_1(a\xi)|^2 \frac{da}{a} = 1$, *for a.e.* $\xi \in \mathbb{R}$;
- $\hat{\psi}_2 \in C_c^\infty(\mathbb{R})$, *supp* $\hat{\psi}_2 \subset [-\frac{\sqrt{2}}{4}, \frac{\sqrt{2}}{4}]$, *is even, nonnegative, decreasing in* $[0, \frac{\sqrt{2}}{4})$, *and* $\|\psi_2\|_2 = 1$.

(i) *If $p_0 \notin \partial S$ then, for all $s \in \mathbb{R}$,*

$$\lim_{a\to 0^+} a^{-N} \mathcal{SH}_\psi B(a, s, p_0) = 0, \quad \text{for all } N > 0.$$

(ii) *If $p_0 \in \partial S$ is a regular point, s does not correspond to the normal direction of ∂S at p_0, then*

$$\lim_{a\to 0^+} a^{-N} \mathcal{SH}_\psi B(a, s, p_0) = 0, \quad \text{for all } N > 0.$$

(iii) *If $p_0 \in \partial S$ is a regular point, s_0 corresponds to the normal direction of ∂S at p_0, and ∂S is k-flat at p_0, then*

$$0 < \lim_{a\to 0^+} a^{-(\frac{1}{2}+\frac{1}{k})} |\mathcal{SH}_\psi B(a, s_0, p_0)| < \infty.$$

(iv) *If $p_0 \in \partial S$ is a regular point, s_0 corresponds to the normal direction of ∂S at p_0 and ∂S is linear near p_0, then*

$$0 < \lim_{a\to 0^+} a^{-\frac{1}{2}} |\mathcal{SH}_\psi B(a, s_0, p_0)| < \infty.$$

Statement (iv) of Theorem 1 can be seen a limiting case of statement (iii), obtained by taking the limit as $k \to \infty$, when ∂S is linear near p_0.

Remark 1 Theorem 1 shows that the continuous shearlet transform $\mathcal{SH}_\psi$ not only identifies through its asymptotic decay as $a \to 0$ the location and local orientation

of an edge, but also its local flatness. If, for example, $Q \in \partial S$ and ∂S is linear near Q (that is, $k = \infty$) then by statement (iv), for $s = s_Q$ corresponding to the normal orientation to ∂S at Q, the function $\mathcal{SH}_\psi B(a, s_Q, Q)$ has slow asymptotic decay as $(a^{1/2})$. If instead $P \in \partial S$ and ∂S is an arc of a circle near P (that is, $k = 1/2$) then by statement (iii), for $s = s_P$ corresponding to the normal orientation to ∂S at P, the function $\mathcal{SH}_\psi B(a, s_P, P)$ has slow asymptotic decay as (a^1).
The microlocal properties of the continuous shearlet transform are confirmed by a simple numerical experiment illustrated in Fig. 2, showing that the decay observed for the discrete shearlet transform at representative edge points located at the boundary of a disk and the side of a rectangular region are consistent with the predictions of Theorem 1. A more detailed investigation of the implication of Theorems 1 and 2 in discrete applications is beyond the scope of this paper and will be addressed in a separate work.

Theorem 2 *Let B, ψ_1, ψ_2 be chosen as in Theorem 1.*

(i) *If $p_0 \in \partial S$ is a corner point of the first type and s does not correspond to any of the normal directions of ∂S at p_0, then*

$$\lim_{a \to 0^+} a^{-\frac{5}{2}} |\mathcal{SH}_\psi B(a, s, p_0)| < \infty.$$

(ii) *If $p_0 \in \partial S$ is a corner point of the second type and s does not correspond to any of the normal directions of ∂S at p_0, then*

$$0 < \lim_{a \to 0^+} a^{-\frac{5}{2}} |\mathcal{SH}_\psi B(a, s, p_0)| < \infty.$$

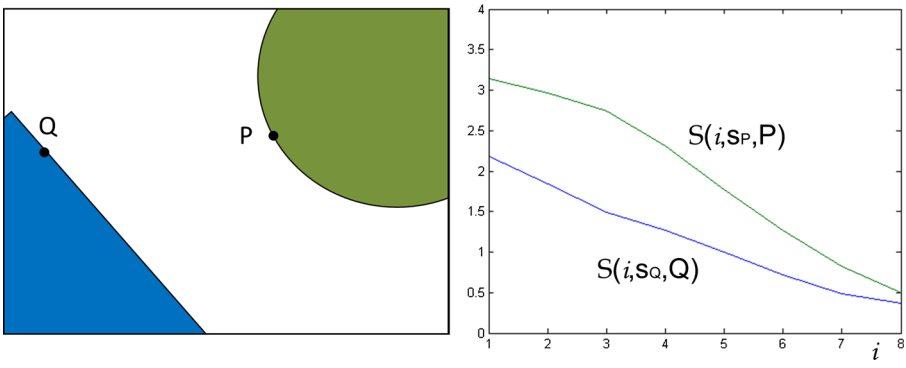

Fig. 2 Decay of the discrete shearlet transform for linear and circular edges. The plot in the *right panel* shows the magnitude of the discrete shearlet transform $S(i, s, p) = |\mathcal{SH}_\psi(2^{-i}, s, p)|$ for points P and Q located, respectively, on the boundary of a disk and of a rectangular region (shown in the *left panel*), as a function of the index i. The symbols s_P and s_Q denote the shear variable for orientations perpendicular to the edge at P and Q, respectively. As i increases (corresponding to finer scales as 2^{-i} becomes smaller), the decay rate of $S(i, s_P, P)$ is faster than $S(i, s_Q, Q)$, as predicted by Theorem 1

(iii) *Let $p_0 \in \partial S$ be a corner point of the first type. Assume that $s = s_0$ corresponds to say the right (resp. left) normal direction of ∂S at p_0 and ∂S is right- (resp. left-) k-flat at p_0 with $2 \le k \le \infty$. Then*

$$0 < \lim_{a \to 0^+} a^{-(\frac{1}{2}+\frac{1}{k})} |\mathcal{SH}_\psi B(a, s_0, p_0)| < \infty.$$

(iv) *Let $p_0 \in \partial S$ be a corner point of the second type and suppose that ∂S is left-k_1-flat and right-k_2-flat at p_0, with $2 \le k_1, k_2 \le \infty$. Let $k = \max\{k_1, k_2\}$. If $s = s_0$ corresponds to one of the normal directions of ∂S at p_0, then*

$$0 < \lim_{a \to 0^+} a^{-(\frac{1}{2}+\frac{1}{k})} |\mathcal{SH}_\psi B(a, s_0, p_0)| < \infty,$$

For brevity, statements (iii) and (iv) of Theorem 2 contain the limiting case $k \to \infty$, when ∂S is linear near p_0. It is understood that, for $k = \infty$, we have $\frac{1}{2} + \frac{1}{k} = \frac{1}{2}$.

3.4 Proof of Theorem 1

The proof requires several steps and its general organization follows the proof in [9]. First, we apply the divergence theorem to write the Fourier transform of $B = \chi_S$ as a line integral over ∂S. Next, we use a localization result to show that the estimates of the integral transform $\mathcal{SH}_\psi B(a, s, p)$ only depend on the values of the integral near p. Finally, we analyze the localized integral for different values of the shear variable s. The easier parts (i)-(ii) of the proof are very similar to the argument in [9] and will not be repeated. Parts (iii) and (iv) of the proof are most critical for the result as they show the lower bound for the estimate at the edge point. Here we use original arguments never appeared before.

3.4.1 Divergence theorem and localization lemma

Using the divergence theorem, we can express the Fourier transform of B as a line integral:

$$\begin{aligned} \hat{B}(\xi) &= \widehat{\chi_S}(\xi) = -\frac{1}{2\pi i |\xi|} \int_{\partial S} e^{-2\pi i \xi \cdot x}\, \Theta(\theta) \cdot \mathbf{n}(x)\, d\sigma(x) \\ &= -\frac{1}{2\pi i \rho} \int_0^L e^{-2\pi i \rho\, \Theta(\theta)\cdot \boldsymbol{\alpha}(t)}\, \Theta(\theta) \cdot \mathbf{n}(t)\, dt \end{aligned} \tag{5}$$

where $\xi = \rho\, \Theta(\theta)$, $\Theta(\theta) = (\cos\theta, \sin\theta)$. Using Eq. 5, we have that

$$\begin{aligned} &\mathcal{SH}_\psi B(a, s, p) \\ &= \langle B, \psi_{a,s,p} \rangle \\ &= \int_0^{2\pi} \int_0^\infty \hat{B}(\rho, \theta)\, \overline{\hat{\psi}^{(d)}_{a,s,p}}(\rho, \theta)\, \rho\, d\rho\, d\theta \\ &= -\frac{1}{2\pi i} \int_0^{2\pi} \int_0^\infty \int_0^L \overline{\hat{\psi}^{(d)}_{a,s,p}}(\rho, \theta) e^{-2\pi i \rho\, \Theta(\theta)\cdot \boldsymbol{\alpha}(t)}\, \Theta(\theta) \cdot \mathbf{n}(t)\, dt\, d\rho\, d\theta, \end{aligned} \tag{6}$$

where the upper-script in $\psi^{(d)}_{a,s,p}$ is either $d = h$, when $|s| \leq 1$, or $d = v$, when $|s| > 1$.

For $\epsilon > 0$, let $D(\epsilon, p)$ be the ball in $\mathbb{R}^2$ of radius ϵ and center p, and $D^c(\epsilon, p) = \mathbb{R}^2 \setminus D(\epsilon, p)$. Hence, using Eq. 6, we can write the shearlet transform of B as

$$\mathcal{SH}_\psi B(a, s, p) = I_1(a, s, p) + I_2(a, s, p),$$

where

$$I_1(a, s, p) = -\frac{1}{2\pi i}\int_0^{2\pi}\int_0^{\infty}\int_{\partial S \cap D(\epsilon,p)} \overline{\hat{\psi}^{(d)}_{a,s,p}}(\rho, \theta) e^{-2\pi i \rho\, \Theta(\theta)\cdot \boldsymbol{\alpha}(t)} \Theta(\theta) \cdot \mathbf{n}(t)\, dt\, d\rho\, d\theta, \quad (7)$$

$$I_2(a, s, p) = -\frac{1}{2\pi i}\int_0^{2\pi}\int_0^{\infty}\int_{\partial S \cap D^c(\epsilon,p)} \overline{\hat{\psi}^{(d)}_{a,s,p}}(\rho, \theta) e^{-2\pi i \rho\, \Theta(\theta)\cdot \boldsymbol{\alpha}(t)} \Theta(\theta) \cdot \mathbf{n}(t)\, dt\, d\rho\, d\theta. \quad (8)$$

The following result shows that I_2 has rapid decay as $a \to 0$. Its proof can be found in [9].

Lemma 1 (Localization Lemma) *Let $I_2(a, s, p)$ be given by* Eq. 8. *For any positive integer N, there is a constant $C_N > 0$ such that*

$$|I_2(a, s, p)| \leq C_N\, a^{\frac{N}{2}},$$

asymptotically as $a \to 0$, uniformly for all $s \in \mathbb{R}$.

We can now proceed with the proof of Theorem 1.

Let $\boldsymbol{\alpha}(t)$ be the boundary curve ∂S, with $0 \leq t \leq L$ and $p_0 \in \partial S$. Since p_0 is a regular point, we can assume without loss of generality that $p_0 = \boldsymbol{\alpha}(1)$ and write the boundary curve near p_0 as $\mathcal{C} = \partial S \cap D(\epsilon, (0, 0))$, where

$$\mathcal{C} = \{\boldsymbol{\alpha}(t) : 1 - \epsilon < t < 1 + \epsilon\}.$$

Rather than using the arclength representation of $\mathcal{C}$, we can also write the curve $\mathcal{C}$ as $\{(G(u), u),\ -\epsilon < u < \epsilon\}$ or $\{(u, G(u)),\ -\epsilon < u < \epsilon\}$, where $G(u)$ is a smooth function. Since the two parametrizations can be handled in a very similar way (by interchanging the role of horizontal and vertical shearlets), in the following we will only consider the form $\mathcal{C} = \{(G(u), u),\ -\epsilon < u < \epsilon\}$. Furthermore, via a translation and rotation of the coordinates, we may assume $p_0 = (0, 0)$ that $\mathcal{C}$ has horizontal tangent at p_0, so that $G(0) = 0$ and $G'(0) = 0$.

We notice that, if G is linear in a nighborhood of p_0, then $G = 0$ in the modified coordinates. In this case ∂S is ∞-flat at p_0. If G is not linear near p_0, since $G(u)$ is of finite type, in the modified coordinate system we have $G(u) = A_k u^k + O(u^{k+1})$ with $A_k \neq 0$ for some $k \geq 2$. In this case, ∂S is k-flat at p_0.

It is sufficient to examine the case of the horizontal shearlets only; the case of vertical shearlets is similar.

- *Parts (i)–(ii).* The proof of these cases is essentially identical to the proof of parts (i)–(ii) of Theorem 3.1 in [9], after replacing $\beta = \frac{1}{2}$ with $\beta = 0$. This proof follows from Lemma 1.

- *Part (iii).* We have that $p_0 = (0,0)$ and $s_0 = 0$, so that $\tan\theta_0 = 0$ (since $G'(0) = 0$). It follows that $G(u) = A_k u^k + O(u^{k+1})$ near $u = 0$ with $A_k \neq 0$ for some $k \geq 2$. By Lemma 1, we need to estimate the integral I_1 at $s_0 = 0$, $p_0 = (0,0)$. In the following when no confusion will occur, for brevity we will simply denote p_0 as 0. Using polar coordinates, we can express $I_1(a,0,0)$ as

$$\begin{aligned} &I_1(a,0,0)\\ &= -\frac{a^{-\frac{1}{2}}}{2\pi i}\int_0^\infty\int_0^{2\pi} \hat\psi_1(\rho\cos\theta)\hat\psi_2(a^{-1}\tan\theta)\int_{-\epsilon}^{\epsilon} e^{-2\pi i\frac{\rho}{a}\cos\theta(A_k u^k+O(u^{k+1}))+\sin\theta\, u}\\ &\quad\times(-\cos\theta+\sin\theta\, O(u^{k-1})\,du\,d\theta\,d\rho. \end{aligned}$$

By Lemma 1, to complete the proof of this case it is sufficient to show that

$$0 < \lim_{a\to 0^+} a^{-(\frac{1}{2}+\frac{1}{k})}\,|I_1(a,0,0)| < \infty.$$

In the expression of I_1, the interval $[0,2\pi]$ of the integral in θ can be broken into the subintervals $[-\frac{\pi}{2},\frac{\pi}{2}]$ and $[\frac{\pi}{2},\frac{3\pi}{2}]$. On $[\frac{\pi}{2},\frac{3\pi}{2}]$, we let $\theta' = \theta - \pi$ so that $\theta' \in [-\frac{\pi}{2},\frac{\pi}{2}]$ and $\sin\theta = -\sin\theta'$, $\cos\theta = -\cos\theta'$. Using this observation and the fact that $\hat\psi_1$ is an odd function, it follows that $I_1(a,0,0) = I_{10}(a,0,0) + I_{11}(a,0,0)$, where

$$\begin{aligned} &2\pi i\, a^{\frac{1}{2}} I_{10}(a,0,0)\\ &= \cos\theta\int_0^\infty\int_{-\frac{\pi}{2}}^{\frac{\pi}{2}} G(\rho,a,\theta)\int_{-\epsilon}^{\epsilon} e^{-2\pi i\frac{\rho}{a}(\cos\theta(A_k u^k+O(u^{k+1}))+u\sin\theta)}du\,d\theta\,d\rho\\ &\quad+\cos\theta\int_0^\infty\int_{-\frac{\pi}{2}}^{\frac{\pi}{2}} G(\rho,a,\theta)\int_{-\epsilon}^{\epsilon} e^{2\pi i\frac{\rho}{a}(\cos\theta(A_k u^k+O(u^{k+1}))+u\sin\theta)}\,du\,d\theta\,d\rho, \end{aligned}$$

$$\begin{aligned} &2\pi i\, a^{\frac{1}{2}} I_{11}(a,0,0)\\ &= -\sin\theta\int_0^\infty\int_{-\frac{\pi}{2}}^{\frac{\pi}{2}} G(\rho,a,\theta)\int_{-\epsilon}^{\epsilon} e^{-2\pi i\frac{\rho}{a}(\cos\theta(A_k u^k+O(u^{k+1}))+u\sin\theta)}O(u^{k-1})du\,d\theta\,d\rho\\ &\quad-\sin\theta\int_0^\infty\int_{-\frac{\pi}{2}}^{\frac{\pi}{2}} G(\rho,a,\theta)\int_{-\epsilon}^{\epsilon} e^{2\pi i\frac{\rho}{a}(\cos\theta(A_k u^k+O(u^{k+1}))+u\sin\theta)}O(u^{k-1})\,du\,d\theta\,d\rho, \end{aligned}$$

and $G(\rho,a,\theta) = \hat\psi_1(\rho\cos\theta)\hat\psi_2(a^{-1}\tan\theta)$.

For $\theta \in (-\frac{\pi}{2},\frac{\pi}{2})$, let $t = a^{-1}\tan\theta$ and $u = a^{\frac{1}{k}}v$. Using this change of variables and the observation that $a \to 0$ implies $\theta \to 0$, it is easy to see that:

$$\lim_{a\to 0}\frac{1}{a}u\sin\theta = \lim_{a\to 0}\frac{1}{a}a^{1+\frac{1}{k}}tv\,\cos\theta = 0,$$

$$\lim_{a\to 0}\frac{1}{a}\cos\theta(A_k u^k+O(u^{k+1})) = \lim_{a\to 0}\frac{1}{a}\cos\theta[a^{k\frac{1}{k}}A_k v^+ a^{1+\frac{1}{k}}O(v^{k+1})] = A_k v^k.$$

It follows that

$$\begin{aligned}
&\lim_{a\to 0^+} 2\pi i\, a^{-(\frac{1}{2}+\frac{1}{k})} I_{10}(a,0,0)\\
&= \int_0^\infty \hat\psi_1(\rho)\int_{-1}^1 \hat\psi_2(t)\int_{-\infty}^\infty e^{-2\pi i\rho A_k v^k}\,dv\,dt\,d\rho\\
&\quad + \int_0^\infty \hat\psi_1(\rho)\int_{-1}^1 \hat\psi_2(t)\int_{-\infty}^\infty e^{2\pi i\rho A_k v^k}\,dv\,dt\,d\rho\\
&= \int_0^\infty \hat\psi_1(\rho)\int_{-1}^1 \hat\psi_2(t)\int_0^\infty \frac{4}{k}\cos(2\pi\rho A_k u)\,u^{-1+\frac{1}{k}}\,du\,dt\,d\rho\\
&= \frac{2}{k}\gamma(\frac{1}{k})\,|2\pi A_k|^{-\frac{1}{k}}\int_0^\infty \hat\psi_1(\rho)\rho^{-\frac{1}{k}}\,d\rho\int_{-1}^1 \hat\psi_2(t)\,dt > 0,
\end{aligned}$$

where $\gamma(\alpha) = \frac{\pi^{\frac{1}{2}}2^\alpha\Gamma(\frac{\alpha}{2})}{\Gamma(\frac{1}{2}-\frac{\alpha}{2})}$ and $\Gamma(\mu) = \int_0^\infty x^{\mu-1}e^{-x}dx$. In the last equality, we used the fact that $\widehat{|x|^{-1+\alpha}}(\xi) = \gamma(\alpha)(2\pi)^{-\alpha}|\xi|^{-\alpha}$, for $0<\alpha<1$. The positivity of the last expression above follows from the assumptions on $\hat\psi_1$, $\hat\psi_2$.

The integral I_{11}can be analyzed using a similar calculation. However, since there is a factor $O(u^{k-1})$ in the expression of I_{11}, this calculation now yields that

$$\lim_{a\to 0^+} 2\pi i a^{-(\frac{1}{2}+\frac{1}{k})} I_{11}(a,0,0) = 0.$$

Combining this estimate with the estimate for I_{10}, we can conclude that

$$0 < \lim_{a\to 0^+} 2\pi i a^{-(\frac{1}{2}+\frac{1}{k})}|I_1(a,s_0,0)| < \infty.$$

This completes the proof of part (iii).

- *Part (iv).* Since ∂S is ∞-flat at p_0, we have that $G(u) = 0$ for all u in a neighborhood of $u = 0$. We can proceed as in the proof pf part (iii) by using polar coordinates to express $I_1(a,0,0)$ and breaking up the integral as a sum $I_{10}(a,0,0) + I_{11}(a,0,0)$. To analyze the integral I_{10}, we use the change of variable $t = a^{-1}\tan\theta$ (but we use no change of variable for u). Using this change of variable and the observation that

$$\lim_{a\to 0}\frac{1}{a}(u\sin\theta) = \lim_{a\to 0}\frac{1}{a}(atu\cos\theta) = tu$$

it follows that

$$\begin{aligned}
\lim_{a\to 0^+} 2\pi i\, a^{-\frac{1}{2}} I_{10}(a,0,0) &= \int_0^\infty \hat\psi_1(\rho)\int_{-1}^1 \hat\psi_2(t)\int_{-\infty}^\infty e^{-2\pi i\rho v t}\,dv\,dt\,d\rho\\
&\quad + \int_0^\infty \hat\psi_1(\rho)\int_{-1}^1 \hat\psi_2(t)\int_{-\infty}^\infty e^{2\pi i\rho v t}\,dv\,dt\,d\rho\\
&= 2\hat\psi_2(0)\int_0^\infty \frac{\hat\psi_1(\rho)}{\rho}\,d\rho > 0,
\end{aligned}$$

where the positivity of the last expression follows from the assumptions on $\hat{\psi}_1$, $\hat{\psi}_2$. This completes the proof of part (iv).

We can now proceed with the proof of Theorem 2. As in the proof above, parts (i), (ii) are similar to [9], while parts (iii) and (iv) require a new argument.

3.4.2 Proof of Theorem 2

When p_0 is a corner point of ∂S, we can write the boundary curve near p_0 as $\mathcal{C} = \partial S \cap D(\epsilon, (0,0)) = \mathcal{C}^- \cup \mathcal{C}^+$, where

$$\mathcal{C}^- = \{\boldsymbol{\alpha}(t) : 1 - \epsilon < t \leq 1\}, \quad \mathcal{C}^+ = \{\boldsymbol{\alpha}(t) : 1 \leq t < 1 + \epsilon\}.$$

Similar to the regular point case, we can express each portion of the curve using a representation of the form $(G(u), u)$ or $(u, G(u))$. Since the two cases can be handled in a very similar way, in the following we will only consider the first one of the two representations. Using an appropriate translation and rotation, we may assume that $p_0 = (0,0)$ and that at least one of the two portions of $\mathcal{C}$ has horizontal tangent at p_0. That is, we write $\mathcal{C}^+ = \{(G^+(u), u),\ 0 \leq u < \epsilon\}$ and $\mathcal{C}^- = \{(G^-(u), u),\ -\epsilon < u \leq 0\}$, where $G^+(u)$ and $G^-(u)$ are smooth functions on $[0, \epsilon)$ and $(-\epsilon, 0]$, respectively. According to the observation above, we may assume $G^+(0) = G^-(0) = 0$ and $(G^+)'(0) = 0$. If p is of the first kind, then $(G^-)'(0) \neq 0$. If p is of the second kind, then $(G^-)'(0) = 0$.

For the remaining of the proof below, it will be sufficient to examine the case of the horizontal shearlets only; the case of vertical shearlets is similar.

- *Parts (i)–(ii).* The proof of these statements follows using the same arguments of the proof of parts (i) and (ii) of Theorem 3.1 in [9], after replacing $\beta = \frac{1}{2}$ with $\beta = 0$.
- *Part (iii).* As argued above, near $p_0 = (0,0)$ we write the boundary curve as $\mathcal{C}^- \cup \mathcal{C}^+$ where $\mathcal{C}^+ = \{(G^+(u), u),\ 0 \leq u \leq \epsilon\}$ and $\mathcal{C}^- = \{(G^-(u), u),\ -\epsilon \leq u \leq 0\}$, and $G^+(u)$ and $G^-(u)$ are smooth functions on $[0, \epsilon]$ and $[-\epsilon, 0]$, respectively with $G^-(0) = 0$ and $G^+(0) = 0$. We may assume that $s_0 = 0$ so that $(G^-)'(0) = 0$, or $(G^+)'(0) = 0$, but not both.

We will only examine the case corresponding to the right normal direction at p_0, since the case corresponding to the left normal direction at p_0 can be analyzed very similarly.

In this case, we can assume that $(G^+)'(0) = 0$ so that $(G^-)'(0) \neq 0$. From part (i), the $\mathcal{C}^-$ section of the curve yields a higher order of decay than the order of decay given by $\mathcal{C}^+$. Thus, in this case, we only need to examine the curve $G^+(u)$. We consider separate cases depending on k being finite or not (recall that the curve $\mathcal{C}^+$ is right-k-flat at p_0).

Case 1: Suppose that $G^+(u)$ is not linear near 0, so that $2 \leq k < \infty$. The analysis of this case is similar to the proof of part (iii) of Theorem 1. That is, after applying

the localization Lemma, and splitting the integral I_1, given by (7), into $I_{10} + I_{11}$, we only need to estimate I_{10}. This leads to the very similar estimate:

$$\begin{aligned}
&\lim_{a\to 0^+} 2\pi i\, a^{-(\frac{1}{2}+\frac{1}{k})} I_{10}(a,0,0)\\
&= \int_0^\infty \hat\psi_1(\rho) \int_{-1}^1 \hat\psi_2(t) \int_0^\infty e^{-2\pi i\rho A_k v^k}\, dv\, dt\, d\rho\\
&\quad + \int_0^\infty \hat\psi_1(\rho) \int_{-1}^1 \hat\psi_2(t) \int_0^\infty e^{2\pi i\rho A_k v^k}\, dv\, dt\, d\rho\\
&= \int_0^\infty \hat\psi_1(\rho) \int_{-1}^1 \hat\psi_2(t) \int_0^\infty \frac{2}{k} \cos(2\pi\rho A_k u)\, u^{-1+\frac{1}{k}} du\, dt\, d\rho\\
&= \frac{1}{k}\gamma(\frac{1}{k}) |2\pi A_k|^{-\frac{1}{k}} \int_0^\infty \hat\psi_1(\rho)\rho^{-\frac{1}{k}} d\rho \int_{-1}^1 \hat\psi_2(t)\, dt > 0,
\end{aligned}$$

where $\gamma(\alpha) = \frac{\pi^{\frac{1}{2}} 2^\alpha \Gamma(\frac{\alpha}{2})}{\Gamma(\frac{1}{2}-\frac{\alpha}{2})}$ and $\Gamma(\mu) = \int_0^\infty x^{\mu-1}e^{-x}dx$. As in the proof of Theorem 1, the positivity of the last expression follows from the assumptions on $\hat\psi_1$, $\hat\psi_2$.

Case 2: Suppose that $G^+(u)$ is linear near 0 so that $k = \infty$. Now we can follow the argument in the proof of part (iv) of Theorem 1. This leads ultimately to the following estimate of the integral I_{10}:

$$\begin{aligned}
\lim_{a\to 0^+} 2\pi i\, a^{-\frac{1}{2}} I_{10}(a,0,0) &= \int_0^\infty \hat\psi_1(\rho) \int_{-1}^1 \hat\psi_2(t) \int_0^\infty e^{-2\pi i\rho v t}\, dv\, dt\, d\rho\\
&\quad + \int_0^\infty \hat\psi_1(\rho) \int_{-1}^1 \hat\psi_2(t) \int_0^\infty e^{2\pi i\rho v t}\, dv\, dt\, d\rho\\
&= \hat\psi_2(0) \int_0^\infty \frac{\hat\psi_1(\rho)}{\rho}\, d\rho > 0.
\end{aligned}$$

The positivity of the last expression follows from the assumptions on $\hat\psi_1$, $\hat\psi_2$.

- *Part (iv).* As in the proof of part (iii), we can write $\mathcal{C}^+ = \{(G^+(u), u),\ 0 \le u \le \epsilon\}$ and $\mathcal{C}^- = \{(G^-(u), u),\ -\epsilon \le u \le 0\}$, where $G^+(u)$ and $G^-(u)$ are smooth functions on $[0,\epsilon]$ and $[-\epsilon, 0]$, respectively, with $G^-(0) = 0$ and $G^+(0) = 0$. We may also assume that $s_0 = 0$. Hence, since p_0 is a corner point of the second type, we have that $(G^-)'(0) = (G^+)'(0) = 0$. We consider different cases separately depending on the values of the degree of flatness.

Case 1: Suppose that $k_1 = k_2 = 2$. In this case, we can write $G^+(u) = A_2u^2 + O(u^3)$ and $G^-(u) = B_2u^2 + O(u^3)$ with $A_2 \neq 0$, $B_2 \neq 0$. Since p_0 is a corner point of the second type, we must have $A_2 \neq B_2$. As above, we can repeat the argument from the proof of part (iii) of Theorem 1 for both curves $\mathcal{C}^+$ and $\mathcal{C}^-$. The estimate for each curve will yield a limit

$$\lim_{a\to 0^+} 2\pi i\, a^{-1} I_{10}(a,0,0) = C_i > 0, \quad i = 1, 2,$$

where the constant C_1 from $\mathcal{C}^+$ is different from the constant C_2 from $\mathcal{C}^-$. Thus the lower bound constant in this case is $C_1 - C_2 \neq 0$.

Case 2: Suppose that $k_1 \neq k_2$. Assume first that $2 = k_1 < k_2 \leq \infty$ so that $k = \max\{k_1, k_2\} = k_2$. Using again the arguments in the proof of part (iii) of Theorem 1, we can estimate the decay rate associated with each curve $\mathcal{C}^+$ and $\mathcal{C}^-$. This argument shows that that the decay rate a^1 from $\mathcal{C}^+$ is higher than the decay rate $a^{\frac{1}{2}+\frac{1}{k_2}}$ from $\mathcal{C}^-$. Thus altogether the decay rate in this case is $a^{\frac{1}{2}+\frac{1}{k_2}}$.

If $2 = k_2 < k_1 \leq \infty$, we can use the same argument to conclude that the decay rate is $a^{\frac{1}{2}+\frac{1}{k_1}}$. The general case $k_1 \neq k_2$ follows in a similar way.

This finishes the proof of Theorem 2.

4 Shearlet analysis of edges in dimension $n = 3$

The shearlet-based analysis of edges extends naturally to the 3-dimensional setting. If $f = \chi_\Omega$, where $\Omega \subset \mathbb{R}^3$ is a compact set with piecewise smooth boundary, it was shown that the 3D shearlet transform $\mathcal{SH}_\psi f$ has 'slow' asymptotic decay at fine scales when the location variable p is at the boundary of Ω and the shear variables correspond to the normal orientation of the boundary at p; for all other cases, $\mathcal{SH}_\psi f$ has rapid asymptotic decay at fine scales [10, 11]. In this section, we show that, similar to the 2-dimensional setting, it is possible to define a variant of the shearlet transform that is able not only to detect the boundary points, but also to identify the flatness of the surface boundary. Since the arguments are similar to the 2D case, in the following we will only present a result for a solid region with smooth boundary. The case of piecewise regular boundaries can be derived by adapting the ideas of the 2-dimensional case.

4.1 Continuous shearlets in $\mathbb{R}^3$

Let us briefly recall the definition of the 3-dimensional continuous shearlet transform. Similar to the 2-dimensional case, for a fixed $\beta = (\beta_1, \beta_2)$, with $0 < \beta_1, \beta_2 < 1$, we define the pyramid-based shearlet systems generated by $\psi^{(d)}, \in L^2(\mathbb{R}^3)$, for $d = \{1, 2, 3\}$, as the functions

$$\{\psi^{(d)}_{a,s,p}(x) = |\det M^{(d)}_{as}|^{-\frac{1}{2}} \psi^{(d)}((M^{(d)}_{as})^{-1}(x-p)) : a > 0, s = (s_1, s_2) \in \mathbb{R}^2, p \in \mathbb{R}^3\},$$

where

$$M^{(1)}_{as} = \begin{pmatrix} a & -a^{\beta_1} s_1 & -a^{\beta_2} s_2 \\ 0 & a^{\beta_1} & 0 \\ 0 & 0 & a^{\beta_2} \end{pmatrix}, \quad M^{(2)}_{as} = \begin{pmatrix} a^{\beta_1} & 0 & 0 \\ -a^{\beta_1} s_1 & a & -a^{\beta_2} s_2 \\ 0 & 0 & a^{\beta_2} \end{pmatrix}, \quad M^{(3)}_{as} = \begin{pmatrix} a^{\beta_1} & 0 & 0 \\ 0 & a^{\beta_2} & 0 \\ -a^{\beta_1} s_1 & -a^{\beta_2} s_2 & a \end{pmatrix}.$$

For $\xi = (\xi_1, \xi_2, \xi_3) \in \mathbb{R}^3$, $\xi_1 \neq 0$, we choose generators $\psi^{(d)}$, $d = 1, 2, 3$, such that

$$\begin{aligned}
\hat{\psi}^{(1)}(\xi) &= \hat{\psi}^{(1)}(\xi_1, \xi_2, \xi_3) = \hat{\psi}_1(\xi_1)\, \hat{\psi}_2(\frac{\xi_2}{\xi_1}), \hat{\psi}_2(\frac{\xi_3}{\xi_1}),\\
\hat{\psi}^{(2)}(\xi) &= \hat{\psi}^{(2)}(\xi_1, \xi_2, \xi_3) = \hat{\psi}_1(\xi_2)\, \hat{\psi}_2(\frac{\xi_1}{\xi_2}), \hat{\psi}_2(\frac{\xi_3}{\xi_2}),\\
\hat{\psi}^{(3)}(\xi) &= \hat{\psi}^{(3)}(\xi_1, \xi_2, \xi_3) = \hat{\psi}_1(\xi_3)\, \hat{\psi}_2(\frac{\xi_2}{\xi_3}), \hat{\psi}_2(\frac{\xi_1}{\xi_3}),
\end{aligned}$$

where ψ_1, ψ_2 satisfy the same assumptions as in the 2D case.

Similar to the 2D case, the continuous shearlets $\psi^{(d)}_{a,s,p}$ are well localized waveforms associated with various scales controlled by a, orientations controlled by the two shear variables s_1, s_2 and locations controlled by p. These properties are more visible in the Fourier domain. For example, the shearlets $\psi^{(1)}_{a,s_1,s_2,p}$ have the form:

$$\hat{\psi}^{(1)}_{a,s_1,s_2,p}(\xi) = a^{\frac{1+\beta_1+\beta_2}{2}}\, \hat{\psi}_1(a\,\xi_1)\, \hat{\psi}_2(a^{\beta_1-1}(\frac{\xi_2}{\xi_1} - s_1))\, \hat{\psi}_2(a^{\beta_2-1}(\frac{\xi_3}{\xi_1} - s_2))\, e^{-2\pi i \xi \cdot p},$$

showing that their Fourier support are contained in trapezoidal regions with scales and orientations controlled by a and $s = (s_1, s_2)$, respectively.

For $f \in L^2(\mathbb{R}^3)$, we define the *3D (fine-scale) pyramid-based continuous shearlet transform* $f \to \mathcal{SH}_\psi f(a, s_1, s_2, p)$, for $a > 0$, $s_1, s_2 \in \mathbb{R}$, $p \in \mathbb{R}^3$ by

$$\mathcal{SH}_\psi f(a, s_1, s_2, p) = \begin{cases} \langle f, \psi^{(1)}_{a,s_1,s_2,p} \rangle & \text{if } |s_1|, |s_2| \leq 1,\\ \langle f, \psi^{(2)}_{a,\frac{1}{s_1},\frac{s_2}{s_1},p} \rangle & \text{if } |s_1| > 1, |s_2| \leq |s_1|\\ \langle f, \psi^{(3)}_{a,\frac{s_1}{s_2},\frac{1}{s_2},p} \rangle & \text{if } |s_2| > 1, |s_2| > |s_1|. \end{cases}$$

Note that, depending on the values of the shearing variables, the 3D continuous shearlet transform only involves one specific pyramid-based shearlet system.

As in the 2D case, for the geometric analysis of edge points conducted in this paper, we will not choose $\beta = (\beta_1, \beta_2) = (\frac{1}{2}, \frac{1}{2})$, corresponding to parabolic scaling, as this choice leads to a transform which can only detect the location and orientation of the edge points, but cannot detect the flatness of the boundary surface. Instead, we choose the special anisotropic scaling parameters $\beta^{(1)} = (0, 1)$ and $\beta^{(2)} = (1, 0)$. Corresponding to $\beta^{(1)}$, for example, the continuous shearlets in the first pyramidal region have the following expression in the Fourier domain:

$$\hat{\psi}^{(1,1)}_{a,s,p}(\xi_1, \xi_2, \xi_3) = a\hat{\psi}_1(a\,\xi_1)\, \hat{\psi}_2(a^{-1}(\frac{\xi_2}{\xi_1} - s_1))\, \hat{\psi}_2(\frac{\xi_3}{\xi_1} - s_2)\, e^{-2\pi i \xi \cdot p}, \quad (9)$$

where the upper index $(1, 1)$ refers to $d = 1$ and $\beta = \beta^{(1)}$. Similarly, for $\beta^{(2)}$, the continuous shearlets in the first pyramidal region have the following expression in the Fourier domain:

$$\hat{\psi}^{(1,2)}_{a,s,p}(\xi_1, \xi_2, \xi_3) = a\hat{\psi}_1(a\,\xi_1)\, \hat{\psi}_2(\frac{\xi_2}{\xi_1} - s_1)\, \hat{\psi}_2(a^{-1}(\frac{\xi_3}{\xi_1} - s_2))\, e^{-2\pi i \xi \cdot p}.$$

Similarly we define $\psi^{(2,1)}_{a,s,p}$, $\psi^{(2,2)}_{a,s,p}$, $\psi^{(3,1)}_{a,s,p}$ and $\psi^{(3,2)}_{a,s,p}$. Corresponding to these two possible choices $\beta^{(i)}$, $i = 1, 2$, we have two distinct versions of the 3D (fine-scale) pyramid-based continuous shearlet transform

$$f \to \mathcal{SH}^{(i)}_{\psi} f(a, s, p), \quad i = 1, 2.$$

We will apply both transforms to derive our main result in the next section.

4.2 Shearlet analysis of surface boundaries

As a model of a 3-dimensional objects, we consider functions of the form $f = \chi_\Omega$, where $\Omega \subset \mathbb{R}^3$ is compact and its boundary $\partial\Omega$ is a 2-dimensional smooth manifold. We denote the outer normal vector at $p_0 \in \partial\Omega$ by

$$\mathbf{n}(p_0) = (\cos\theta_0 \sin\phi_0, \sin\theta_0 \sin\phi_0, \cos\phi_0),$$

for some angles $\theta_0 \in [0, 2\pi]$, $\phi_0 \in [0, \pi]$. Similar to the 2D case, we say that $s = (s_1, s_2)$ corresponds to the normal direction $\mathbf{n}(p_0)$ if $s_1 = \tan\theta_0$ and $s_2 = \cot\phi_0 \sec\theta_0$.

Given a point $p = (p_1, p_2, p_3) \in \partial\Omega$ and a neighborhood of p in $\partial\Omega$, there are three possible parametrizations of the surface in this neighborhood:

$$\Sigma_1 = \{(G(u), u_2, u_3),\ (u_2, u_3) \in O_1\},\ \text{or}\ \ \Sigma_2 = \{(u_1, G(u), u_3),\ (u_1, u_3) \in O_2\}$$

$$\text{or}\ \ \Sigma_3 = \{(u_1, u_2, G(u_1, u_2)),\ (u_1, u_2) \in O_3\},$$

where O_1 is a neighborhood of (p_2, p_3) in yz plane, O_2 is a neighborhood of (p_1, p_3) in xz plane and O_3 is a neighborhood of (p_1, p_2) in xy plane. To define a notion of *flatness* in the 3-dimensional setting, we refer below to the parametrization Σ_1, but it is easy to extend the same idea to Σ_2 and Σ_3.

For $p \in \Sigma_1$, if G is not linear near p, we assume that there exists $2 \le k < \infty$ such that by a translation and a rotation of the coordinates if necessary, we have $p = (0, 0, 0)$ so that near $(0, 0)$, we have $G(u_2, u_3) = A_k u_2^k + B_k u_3^k + A_1(u_2)u_3 + A_2(u_2)u_3^2 + \cdots + A_{k-1}(u_2)u_3^{k-1} + O(|u_3|^{k+1})$ or $G(u_2, u_3) = A_k u_2^k + B_k u_3^k + B_1(u_3)u_2 + B_2(u_3)u_2^2 + \cdots + B_{k-1}(u_3)u_2^{k-1} + O(|u_2|^{k+1})$.

If there is a $2 \le k < \infty$ such that $A_k \neq 0$ or $B_k \neq 0$, then we say $\partial\Omega$ is *k-flat* at p or that its degree of flatness is k at p. If G is linear near p, then $G = 0$ under the new coordinates and in this case we say that $\partial\Omega$ is ∞-*flat* at p, as for the 2-dimensional case. There is still one possible situation to consider, where there is a $2 \le k < \infty$ such that $A_k = 0$ and $B_k = 0$. In this case we say that $\partial\Omega$ is *overflat* at p. When $A_k = 0$, the projection of the surface Σ_1 onto xy plane is a curve that is k-flat at (0,0), while $B_k = 0$ means that the projection of the surface Σ_1 onto xz plane is a k-flat curve at (0,0). When $\partial\Omega$ is *overflat* at p, then projection of the surface Σ_1 onto xz plane is a k-flat curve at (0,0). When $\partial\Omega$ is *overflat* at p, then projection of the surface Σ_1 onto xy plane is a segment of y axis and the projection of the surface Σ_1 onto xz plane is a segment of z axis, which are ∞-flat at $(0, 0)$ for both curves. Thus it is no surprise to see that the decay rate for the case of *overflat* is the same for the case of ∞-*flat*.

The following Theorem shows that the continuous shearlet transform characterizes the geometry of the boundary set $\partial\Omega$, including its local flatness. Note that, unlike the corresponding 2-dimensional result in Section 3, in this case we need to use two versions of the shearlet transform, i.e., $\mathcal{SH}_\psi^{(1)}$ and $\mathcal{SH}_\psi^{(2)}$, for different values of the anisotropy parameter β.

Theorem 3 *Let $f = \chi_\Omega$ be as above and ψ_1 ψ_2 be chosen as in Theorem 1.*

(i) *If $p_0 \notin \partial\Omega$ then, for $i = 1$ or $i = 2$,*

$$\lim_{a\to 0^+} a^{-N}\, \mathcal{SH}_\psi^{(i)} f(a, s, p_0) = 0, \quad \text{for all } N > 0.$$

(ii) *If $p_0 \in \partial\Omega$ and $s = (s_1, s_2)$ does not correspond to the normal direction of $\partial\Omega$ at p, then, for $i = 1$ or $i = 2$,*

$$\lim_{a\to 0^+} a^{-N}\, \mathcal{SH}_\psi^{(i)} f(a, s, p_0) = 0, \quad \text{for all } N > 0.$$

(iii) *If $p_0 \in \partial\Omega$, $\partial\Omega$ is k-flat at p_0, with $2 < k < \infty$), and $s = (s_1, s_2)$ correspond to the normal direction of $\partial\Omega$ at p_0, then either*

$$0 < \lim_{a\to 0^+} a^{-(1+\frac{1}{k})}\, |\mathcal{SH}_\psi^{(1)} f(a, s, p_0)| < \infty$$

or

$$0 < \lim_{a\to 0^+} a^{-(1+\frac{1}{k})}\, |\mathcal{SH}_\psi^{(2)} f(a, s, p_0)| < \infty$$

(iv) *If $p \in \partial\Omega$, $\partial\Omega$ is overflat at p_0 and $s = (s_1, s_2)$ corresponds to the normal direction of $\partial\Omega$ at p_0, then*

$$\lim_{a\to 0^+} a^{-1}\, |\mathcal{SH}_\psi^{(1)} f(a, s, p_0)| < \infty \quad \text{and} \quad \lim_{a\to 0^+} a^{-1}\, |\mathcal{SH}_\psi^{(2)} f(a, s, p_0)| < \infty$$

(v) *If $p_0 \in \partial\Omega$, $\partial\Omega$ is ∞-flat at p_0 and $s = (s_1, s_2)$ corresponds to the normal direction of $\partial\Omega$ at p_0, then*

$$0 < \lim_{a\to 0^+} a^{-1}\, |\mathcal{SH}_\psi^{(1)} f(a, s, p_0)| < \infty \quad \text{and} \quad 0 < \lim_{a\to 0^+} a^{-1}\, |\mathcal{SH}_\psi^{(2)} f(a, s, p_0)| < \infty$$

Proof The proof follows the main architecture of the proof of Theorem 1, that is: (1) we apply the divergence theorem (in 3D) to write the Fourier transform of f as a surface integral over $\partial\Omega$; (2) we use the localization properties of shearlets to write the shearlet transform $\mathcal{SH}_\psi^{(i)} f(a, s, p)$ as a sum $I_1(a, s, p) + I_2(a, s, p)$, where I_1 depends by the values of the integrals near p and I_2 depends by the values of the integrals away p; (3) since I_2 decays rapidly as $a \to 0$, the asymptotic decay rate of $\mathcal{SH}_\psi^{(i)} f(a, s, p)$, as $a \to 0$, is completely controlled by the asymptotic decay rate of the integral $I_1 a, s, p)$, as $a \to 0$. Steps (1) and (2) above are the same as in Theorem 3.1 in [11] and will not be repeated here. Thus, in the arguments below, we only discuss how to analyze the integrals

$$I_1(a, s_1, s_2, p) = \int_0^{2\pi}\int_0^{\pi}\int_0^{\infty} T_1(\rho, \theta, \phi)\, \overline{\hat{\psi}^{(d)}_{a,s_1,s_2,p}}(\rho, \theta, \phi)\, \rho^2 \sin\phi\, d\rho\, d\phi\, d\theta,$$

where

$$T_1(\rho,\theta,\phi) = -\frac{1}{2\pi i\rho}\int_{\partial\Omega\cap D(\epsilon,p)} e^{-2\pi i\rho\,\Theta(\theta,\phi)\cdot x}\,\Theta(\theta,\phi)\cdot\mathbf{n}(x)\,d\sigma(x)$$

and $D(\epsilon,\,p)$ is the ball in $\mathbb{R}^3$ of radius ϵ and center p. It is understood that, if needed, one can replace the set $\partial\Omega\cap D(\epsilon,\,p)$ with a rectangular neighbourhood of $(p_2,\,p_3)$ in yz plane: $\{(u_1,u_2):\ |u_1-p_2|<\epsilon, |u_2-p_3|<\epsilon\}$.

As in the 2-dimensional case, for $p\in\partial\Omega$, via translation and rotation we can change coordinates so that $p_0=(0,0,0)$ and the tangent plane to the surface $\partial\Omega$ at p_0 is the plane $z=0$. As in the 2D case, we can represent the surface $\partial\Omega$ near p_0 using the three possible parametrizations Σ_i, $i=1,2,3$, indicated above. It will be sufficient to consider only the parametrization $\Sigma_1=\{(G(u_2,u_3),u_2,u_3),\ (u_2,u_3)\in O_1\}$, where O_1 is a neighborhood of $(0,0)$ in the yz plane, that can be analyzed using the continuous shearlets $\{\psi^{(1,1)}_{a,s,t}\}$ and $\{\psi^{(1,2)}_{a,s,t}\}$ associated with the first pyramidal region. The other cases (involving the parametrization Σ_2 and Σ_3) can be handled using a very similar argument (using the continuous shearlets associated with the other pyramidal regions).

- *Parts (i)–(ii).* The proof of these cases is essentially the same as the proof of parts (i) and (ii) of Theorem 3.1 in [11].
- *Part (iii).* Due to our assumption that $p_0=(0,0,0)$, we have that $G(0,0)=0$. Due to the assumption on the orientation of the surface $\partial\Omega$ near p_0, we have that $s_1=s_2=0$, so that $\theta_0=0$, $\phi_0=\frac{\pi}{2}$ (recall that $s_1=\tan\theta_0$, $s_2=\cot\phi_0\sec\theta_0$). In this setting, we can replace $\partial\Omega\cap D(\epsilon,\,p)$ by $\{(G(u_2,u_3),u_2,u_3):\ |u_1|<\epsilon,|u_2|<\epsilon\}$ in the definition of $T_1(\rho,\theta,\phi)$, where $G(0,0)=G_{u_2}(0,0)=G_{u_3}(0,0)=0$.

  We start by considering the integral I_1 associated with the shearlet transform $\mathcal{SH}^{(1)}_{\psi}$. Under the assumption we made, we have that

$$I_1(a,s_1,s_2,\,p)=\int_0^{2\pi}\int_0^{\pi}\int_0^{\infty} T_1(\rho,\theta,\phi)\,\overline{\hat{\psi}^{(1,1)}_{a,s_1,s_2,p}}(\rho,\theta,\phi)\,\rho^2\sin\phi\,d\rho\,d\phi\,d\theta,$$

  where

$$\begin{aligned}T_1(\rho,\theta,\phi) &= \frac{-1}{2\pi i\rho}\int_{-\epsilon}^{\epsilon}\int_{-\epsilon}^{\epsilon} e^{-2\pi i\rho\,\Theta(\theta,\phi)\cdot(G(u_2,u_3),u_2,u_3))}\Theta(\theta,\phi)\cdot\mathbf{n}(u)\,d\sigma(u)\\ &= \frac{-1}{2\pi i\rho}\int_{-\epsilon}^{\epsilon}\int_{-\epsilon}^{\epsilon} e^{-2\pi i\rho\,\Theta(\theta,\phi)\cdot(G(u_2,u_3),u_2,u_3))}\Theta(\theta,\phi)\cdot(-1,G_{u_2},G_{u_3})du_2du_3.\end{aligned}$$

  By dividing the interval of integration $\theta\in[0,2\pi]$ in the integral I_1 into the two subintervals $[-\frac{\pi}{2},\frac{\pi}{2}]$ and $[\frac{\pi}{2},\frac{3\pi}{2}]$, we can write $I_1=I_{11}+I_{12}$, where I_{11} and I_{12} are the terms in I_1 corresponding to the intervals $[-\frac{\pi}{2},\frac{\pi}{2}]$ and $[\frac{\pi}{2},\frac{3\pi}{2}]$ respectively. It is easy to verify that I_{11} is the complex conjugate of I_{12} and, thus, it will be sufficient to analyze I_{11}.

In $T_1(\rho, \theta, \phi)$, we have that

$$\Theta(\theta, \phi) \cdot (-1, G_{u_2}, G_{u_3}) = -\cos\theta \sin\phi + \sin\theta \sin\phi G_{u_2}(u) + \cos\phi G_{u_3}(u)$$

and the right hand side can be replaced by $-\cos\theta \sin\phi$ since, as the argument below will the term $\sin\theta \sin\phi G_{u_2}(u) + \cos\phi G_{u_3}(u)$ yields a higher order of decay. In fact, due to the assumptions on G, we have that $G_{u_2}(u) = O(|u|)$ and that $G_{u_3}(u) = O(|u|)$.

Using the expression of $\hat{\psi}^{(1,1)}_{a,s,p}$ from Eq. 9, with $p = (0, 0, 0)$, $s_1 = s_2 = 0$) and the change of variable $a\rho \to \rho$, we hence obtain

$$\begin{aligned} & I_{11}(a, 0, 0, 0) \\ = & \frac{1}{2a\pi i} \int_{-\frac{\pi}{2}}^{\frac{\pi}{2}} \int_0^{\pi} \int_0^{\infty} \hat{\psi}_1(\rho \sin\phi \cos\theta) \hat{\psi}_2(a^{-1}(\tan\theta)) \hat{\psi}_2(\cot\phi \sec\theta) \\ & \times \int_{-\epsilon}^{\epsilon} \int_{-\epsilon}^{\epsilon} e^{2\pi i \frac{\rho}{a} \Theta(\theta,\phi) \cdot (G(u_2,u_3), u_2, u_3)} \sin\phi \cos\theta \, du_2 du_3 \, \rho \sin\phi \, d\rho \, d\phi \, d\theta, \end{aligned}$$

where $\Theta(\theta, \phi) = (\sin\phi \cos\theta, \sin\phi \sin\theta, \cos\phi)$.

By the assumption on the flatness, we have either $A_k \neq 0$ or $B_k \neq 0$. Let us consider the two cases separately.

Case $A_k \neq 0$. Under this assumption, we write $G(u_2, u_3)$ as

$$G(u_2, u_3) = A_k u_2^k + B_k u_3^k + A_1(u_2)u_3 + A_2(u_2)u_3^2 + \cdots + A_{k-1}(u_2)u_3^{k-1} + O(|u_3|^{k+1}).$$

In the integral I_{11}, we will use the change of variables $t_1 = a^{-1}(\tan\theta)$, $t_2 = \cot\phi \sec\theta$, $u_2 = a^{\frac{1}{k}} v_1$, and $u_3 = a v_2$. Since $a \to 0$ implies $\theta \to 0$, $\phi \to \frac{\pi}{2}$, we have that

$$\begin{aligned} & \lim_{a\to 0} \frac{1}{a} \cos\theta \sin\phi \, G(u_2, u_3) \\ = & \lim_{a\to 0} \frac{1}{a} \cos\theta \sin\phi \left(A_k u_2^k + B_k u_3^k + A_1(u_2)u_3 + A_2(u_2)u_3^2 + \cdots + A_{k-1}(u_2)u_3^{k-1} \right. \\ & \left. + O(|u_3|^{k+1}) \right) \\ = & \lim_{a\to 0} \frac{1}{a} \cos\theta \sin\phi \left(a A_k v_1^k + a^k B_k u_3^k + a A_1(a^{\frac{1}{k}} v_1) v_2 + a^2 A_2(a^{\frac{1}{k}} v_1) v_2^2 + \cdots \right. \\ & \left. + a^{k-1} A_{k-1}(a^{\frac{1}{k}} v_1) v_2^{k-1} + a^{k+1} O(|v_2|^{k+1}) \right) \\ = & A_k v_1^k \end{aligned}$$

and that

$$\begin{aligned} \lim_{a\to 0} \frac{1}{a} (\sin\theta \sin\phi u_2 + \cos\phi u_3) &= \lim_{a\to 0} \frac{1}{a} \left(a t_1 (a^{\frac{1}{k}} v_1)(\cos\theta \sin\phi) + a t_2 v_2 \cos\theta \right) \\ &= t_2 v_2. \end{aligned}$$

From these observations, it follows that

$$\begin{aligned}
&\lim_{a\to 0^+} a^{-(1+\frac{1}{k})}\mathrm{Re}[\pi i\, I_{11}(a,0,0,0)]\\
&= \int_0^\infty \hat\psi_1(\rho)\,\mathrm{Re}\left[\int_{-\infty}^\infty\int_{-\infty}^\infty\int_{-1}^1\int_{-1}^1 \hat\psi_2(t_1)\hat\psi_2(t_2)e^{2\pi i\rho(A_k v_1^k+v_2t_2)}dt_1dt_2dv_1dv_2\right]\rho d\rho\\
&= \int_0^\infty \hat\psi_1(\rho)\,\mathrm{Re}\left[\int_{-\infty}^\infty\int_{-\infty}^\infty \psi_2(\rho v_1)\psi_2(\rho v_2)dv_1dv_2\right]\rho d\rho\\
&= \int_0^\infty \hat\psi_1(\rho)\,\mathrm{Re}\left[\int_{-\infty}^\infty e^{2\pi i\rho A_k v_1^k}dv_1\int_{-\infty}^\infty \psi_2(\rho v_2)dv_2\right]\int_{-1}^1\hat\psi_2(t_1)dt_1\rho d\rho\\
&= \hat\psi_2^2(0)\int_0^\infty \frac{\hat\psi_1(\rho)}{\rho}\,d\rho \neq 0,
\end{aligned}$$

where the positivity of the last expression follows from the assumptions on $\hat\psi_1$, $\hat\psi_2$. As we observed above, the estimate on I_{11} implies the estimate on $\mathcal{SH}_\psi^{(1,1)}$. In fact, the last limit implies that

$$0 < |\lim_{a\to 0^+} a^{-(1+\frac{1}{k})}\,\mathcal{SH}_\psi^{(1,1)} f(a,s,p_0)| < \infty.$$

Case $B_k \neq 0$. In this case, we write $G(u_2,u_3)$ as

$$G(u_2,u_3) = A_k u_2^k + B_k u_3^k + B_1(u_3)u_2 + B_2(u_3)u_2^2 + \cdots + B_{k-1}(u_3)u_2^{k-1} + O(|u_2|^{k+1}).$$

Then the same argument as above applied to $\mathcal{SH}_\psi^{(1,2)}$ will yield that

$$0 < |\lim_{a\to 0^+} a^{-(1+\frac{1}{k})}\,\mathcal{SH}_\psi^{(1,2)} f(a,s,p_0)| < \infty.$$

This completes the proof of part (iii).

- *Part (iv).* The analysis of $\mathcal{SH}_\psi^{(1,1)} f(a,s,p_0)$ and $\mathcal{SH}_\psi^{(1,2)} f(a,s,p_0)$ is very similar. Thus, we will only present the argument for $\mathcal{SH}_\psi^{(1,1)} f(a,s,p_0)$. As argued above, ultimately this requires to estimate the integral I_{11}.

  Proceeding in a similar way to part (iii), for I_{11} we use the change of variables $t_1 = a^{-1}(\tan\theta)$, $t_2 = \cot\phi\sec\theta$ and $u_2 = v_1,\ u_3 = av_2$. Similar to the proof of part (iii), we have

$$\lim_{a\to 0}\frac{1}{a}\cos\theta\sin\phi G(u_2,u_3) = A_1(v_1)v_2$$

and

$$\lim_{a\to 0}\frac{1}{a}(\sin\theta\sin\phi u_2 + \cos\phi u_3) = t_1v_1 + t_2v_2.$$

Using the change of variables and these limits we have that

$$\begin{aligned}
&\lim_{a\to 0^+}\pi i a^{-1}\mathrm{Re}[I_{11}(a,0,0,0)]\\
&= \int_0^\infty \hat\psi_1(\rho)\mathrm{Re}\left[\int_{-\infty}^\infty\int_{-\infty}^\infty\int_{-1}^1\int_{-1}^1 \hat\psi_2(t_1)\hat\psi_2(t_2)e^{2\pi i\rho(A_1(v_1)v_2+v_1t_1+v_2t_2)}dt_1dt_2dv_1dv_2\right]\rho d\rho\\
&= \int_0^\infty \hat\psi_1(\rho)\mathrm{Re}\left[\int_{-\infty}^\infty\int_{-\infty}^\infty e^{2\pi i\rho A_1(v_1)v_2}\psi_2(\rho v_1)\psi_2(\rho v_2)dv_1dv_2\right]\rho d\rho.
\end{aligned}$$

The right hand side of the last identity is obviously finite. However, we cannot ensure that this quantity is also nonzero, except for the special case $A_1(v_1) = 0$. Hence we cannot derive a lower bound in this case.

One can analyze in a similar way the shearlet transform $\mathcal{SH}_\psi^{(12)} f(a, s, p_0)$, by replacing $A_1(v_1)v_2$ with $B_1(v_2)v_1$. This finishes the proof of part (iv).

- *Proof of part (v).* Again, the analysis of $\mathcal{SH}_\psi^{(1,1)} f(a, s, p_0)$ and $\mathcal{SH}_\psi^{(1,2)} f(a, s, p_0)$ is very similar. Thus, we will only present the argument for $\mathcal{SH}_\psi^{(1,1)} f(a, s, p_0)$.

  As above, the argument reduces ultimately to estimate the integral I_{11}.

  In this case, we use the change of variables $t_1 = a^{-1}(\tan\theta)$, $t_2 = \cot\phi \sec\theta$, $u_2 = v_1$ and $u_3 = av_2$. Since $G(u_2, u_3) = 0$ in this case, we have

$$\begin{aligned}
&\lim_{a\to 0^+} a^{-1}\mathrm{Re}[\pi i\, I_{11}(a, 0, 0, 0)] \\
&= \int_0^\infty \hat{\psi}_1(\rho)\mathrm{Re}\left[\int_{-\infty}^\infty\int_{-\infty}^\infty\int_{-1}^1\int_{-1}^1 \hat{\psi}_2(t_1)\hat{\psi}_2(t_2)e^{2\pi i\rho(v_1t_1+v_2t_2)}dt_1dt_2dv_1dv_2\right]\rho d\rho \\
&= \int_0^\infty \hat{\psi}_1(\rho)\mathrm{Re}\left[\int_{-\infty}^\infty\int_{-\infty}^\infty \psi_2(\rho v_1)\psi_2(\rho v_2)dv_1dv_2\right]\rho d\rho \\
&= \int_0^\infty \hat{\psi}_1(\rho)\mathrm{Re}\left[\int_{-\infty}^\infty\int_{-\infty}^\infty \psi_2(v_1)\psi_2(v_2)dv_1dv_2\right]\rho^{-1}d\rho \\
&= (\hat{\psi}_2(0))^2\int_0^\infty \hat{\psi}_1(\rho)\rho^{-1}d\rho \neq 0.
\end{aligned}$$

This finishes the proof of part (v) and hence the proof of Theorem 3.

□

References

1. Bros, J., Iagolnitzer, D.: Support essentiel et structure analytique des distributions. Seminaire Goulaouic-Lions-Schwartz **19**, 1975–1976 (1976)
2. Candès, E.J., Donoho, D.L.: Continuous curvelet transform: I. Resolution of the wavefront set. Appl. Comput. Harmon. Anal. **19**, 162–197 (2005)
3. Córdoba, A., Fefferman, C.: Wave packets and Fourier integral operators. Communications in Partial Differential Equations **3**(11), 979–1005 (1978)
4. Donoho, D., Kutyniok, G.: Microlocal analysis of the geometric separation problem. Comm. Pure Appl. Math. **66**, 1–47 (2013)
5. Duval-Poo, M.A., Odone, F., De Vito, E.: Edges and corners with shearlets. IEEE Trans. Image Process. **24**(11), 3768–3780 (2015)
6. Easley, G., Labate, D., Lim, W.: Sparse directional image representations using the discrete shearlet transform. Appl. Comput. Harmon. Anal. **25**, 25–46 (2008)
7. Genzel, M., Kutyniok, G.: Asymptotic analysis of inpainting via universal shearlet systems. SIAM J. Imaging Sci. **7**, 2301–2339 (2014)
8. Grohs, P.: Continuous shearlet frames and resolution of the wavefront set. Monatshefte för Mathematik **164**(4), 393–426 (2011)
9. Guo, K., Labate, D.: Characterization and analysis of edges using the continuous shearlet transform. SIAM on Imaging Sciences **2**, 959–986 (2009)

10. Guo, K., Labate, D.: Analysis and detection of surface discontinuities using the 3D continuous shearlet transform. Appl. Comput. Harmon. Anal. **30**, 231–242 (2011)
11. Guo, K., Labate, D.: Characterization of piecewise-smooth surfaces using the 3D continuous shearlet transform. J. Fourier Anal. Appl. **18**, 488–516 (2012)
12. Guo, Labate, D.: Geometric separation of singularities using combined multiscale dictionaries. J. Fourier Anal. Appl. **21**(4), 667–693 (2015)
13. Guo, K., Labate, D.: Characterization and analysis of edges in piecewise smooth functions. Appl. Comput. Harmon. Anal. **41**(1), 139–163 (2016)
14. Guo, K., Labate, D., Lim, W.: Edge analysis and identification using the continuous shearlet transform. Appl. Comput. Harmon. Anal. **27**(1), 24–46 (2009)
15. Guo, K., Houska, R., Labate, D.: Microlocal analysis of singularities from directional multiscale representations. In: Proceedings from: Approximation Theory XIV: San Antonio 2013 (April 7-10, 2013, San Antonio, Texas). Springer Proceedings in Mathematics & Statistics, vol. 83, pp. 173–196 (2014)
16. Holschneider, M.: Wavelets. Analysis tool. Oxford University Press, Oxford (1995)
17. Jaffard, S.: Pointwise smoothness, two-microlocalization and wavelet coefficients. Publications Matematiques **35**, 155–168 (1991)
18. Jaffard, S., Meyer, Y.: Wavelet methods for pointwise regularity and local oscillations of functions. Memoirs of the AMS **123**(587) (1996)
19. King, E., Kutyniok, G., Zhuang, X.: Analysis of inpainting via clustered sparsity and microlocal analysis. J. Math. Imaging Vision **48**(2), 205–234 (2014)
20. Kutyniok, G., Labate, D.: Resolution of the wavefront set using continuous shearlets. Trans. Amer. Math. Soc. **361**, 2719–2754 (2009)
21. Kutyniok, G., Petersen, P.: Classification of edges using compactly supported shearlets. Appl. Comput. Harmon. Anal. (2015). doi:10.1016/j.acha.2015.08.006
22. Kutyniok, G., Shahram, M., Zhuang, X.: Shearlab: a rational design of a digital parabolic scaling algorithm. SIAM J. Imaging Sci. **5**(4), 1291–1332 (2012)
23. Meyer, Y.: Wavelets and Operators, Cambridge Stud. Adv Math, vol. 37. Cambridge University Press, Cambridge (1992)
24. O'Leary, D.P., Schug, D.A., Easley, G.R.: Three-dimensional shearlet edge analysis. In: Proceedings of the SPIE 8058, Independent Component Analyses, Wavelets, Neural Networks, Biosystems, and Nanoengineering IX (2011)
25. Ozcan, B., Negi, P., Laezza, F., Papadakis, M., Labate, D.: Automated detection of soma location and morphology in neuronal network cultures. PLos ONE **10**(4) (2015)
26. Reisenhofer, R., Kiefer, J., King, E.J.: Shearlet-based detection of flame fronts. Exp. Fluids **57**(3), 41:1–41:14 (2016)
27. Yi, S., Labate, D., Easley, G.R., Krim, H.: A shearlet approach to edge analysis and detection. IEEE Trans. Image Process. **18**, 929–941 (2009)